Hindawi Publishing Corporation
Journal of Nanomaterials
Volume 2013, Article ID 741036, 9 pages
http://dx.doi.org/10.1155/2013/741036

Research Article

Magnetic and Structural Studies of $CoFe_2O_4$ Nanoparticles Suspended in an Organic Liquid

Branka Babić-Stojić,[1] Vukoman Jokanović,[1] Dušan Milivojević,[1] Zvonko Jagličić,[2] Darko Makovec,[3] Nataša Jović,[1] and Milena Marinović-Cincović[1]

[1] *Vinča Institute of Nuclear Sciences, University of Belgrade, P.O. Box 522, 11001 Belgrade, Serbia*
[2] *Institute of Mathematics, Physics and Mechanics, Jadranska 19, 1000 Ljubljana, Slovenia*
[3] *Department for Materials Synthesis, Jožef Stefan Institute, Jamova 39, 1000 Ljubljana, Serbia*

Correspondence should be addressed to Branka Babić-Stojić; babic@vinca.rs

Received 16 September 2013; Accepted 17 October 2013

Academic Editor: Haifeng Chen

We present a study of magnetic and structural properties of $CoFe_2O_4$ nanoparticles suspended in an organic liquid. Transmission electron microscopy shows that the nanoparticles have a narrow size distribution of average particle size 5.9 ± 1.0 nm. X-ray diffraction shows that the particles are of cubic spinel crystal structure. Dynamic light scattering measurements reveal the existence of an organic shell around the $CoFe_2O_4$ nanoparticles with an average hydrodynamic diameter of 14.4 nm. Coercive magnetic field at $T = 5$ K is found to be 11.8 kOe. Disappearance of the coercive field and remanent magnetization at about 170 K suggests that the $CoFe_2O_4$ nanoparticles are superparamagnetic at higher temperatures which is confirmed by the room temperature Mössbauer spectrum analysis. Saturation magnetization of the nanoparticles of 80.8 emu/g($CoFe_2O_4$) at 5 K reaches the value detected in the bulk material and remains very high also at room temperature. The cobalt ferrite nanoparticle system synthesized in this work exhibits magnetic properties which are very suitable for various biomedical applications.

1. Introduction

Ferrofluids are stable colloidal suspensions of single domain magnetic particles in a carrier liquid. Stability of the magnetic colloid depends on the thermal contribution and on the balance between attractive and repulsive interactions. Magnetic dipole and van der Waals interactions have tendency to agglomerate the particles. In order to prevent agglomeration, the magnetic particles should be small enough (usually about 10 nm in size) and coated with a shell of an appropriate material. This coating can be a sufactant made of long chained molecules or ionic if it is an electric shell [1–3]. The particles are usually made of maghemite γ-Fe_2O_3, magnetite Fe_3O_4, and other ferrites of the type MFe_2O_4, where M = Mn, Co, Ni, Cu. The carrier liquid is usually an organic solvent or water. Ferrofluids respond to an external magnetic field. This enables the ferrofluid's location to be controlled through the application of a magnetic field. Ferrofluids have a wide range of applications. They can be used to improve the performance of loud speakers [2]. Ferrofluids are also used in high-speed computer disk drives to eliminate harmful dust particles or other impurities that can cause the data-reading heads to crash into the disks. In recent years, a lot of research work has been devoted to biomedical applications of ferrofluids. In magnetic resonance imaging (MRI), ferrofluids are used as contrast agents [3–5]. Ferrofluids specially designed can carry drugs to specific locations in the living body through the use of applied magnetic fields [3, 6]. Heat treatment of organs or tissues called hyperthermia uses the property of ferrofluids of absorbing electromagnetic energy. This allows heating of a localized part of a living body, such as malignant tumor, up to temperature 42–46°C which reduces the viability of cancerous cells [3, 4, 6]. For various applications, particularly in biomedicine, magnetic particles in ferrofluids, besides the requirement for small sizes, must have large enough magnetization. Depending on the relative magnitude of anisotropy energy with respect to thermal energy, the particles exhibit superparamagnetic

behavior when magnetic moment of the particle overcomes the anisotropy energy barrier by thermal activation. For a given temperature T and time τ characteristic to a specific measurement, there is a critical particle diameter D_{sp} (assuming spherical shape) that separates smaller particles $D < D_{sp}$ exhibiting superparamagnetism from larger particles $D > D_{sp}$ which have ferro(ferri)magnetic properties. For cubic magnetocrystalline anisotropy, the energy barrier is $E = KV/4$, where V is the particle volume. The critical size of the $CoFe_2O_4$ particles with anisotropy constant $K = 2 \times 10^6$ erg cm^{-3} at $T = 300$ K [7] and for $\tau = 10^2$ s can be estimated [8] as $D_{sp} \approx 16$ nm. In the case of axial magnetocrystalline anisotropy, the energy barrier is $E = KV$, and, for the same values of the parameters K, T, and τ, the critical particle size is $D_{sp} \approx 10$ nm.

There are two dominant mechanisms of magnetic relaxation in a ferrofluid, the Brownian relaxation and Néel relaxation. When the relaxation is dominated by the Brownian mechanism, the magnetic moment is rotated together with the nanoparticle in the carrier liquid under the influence of an external magnetic field [9]. Relaxation time for the Brownian rotational motion is

$$\tau_B = \frac{3V_h\eta}{k_BT}, \quad (1)$$

where V_h is the hydrodynamic volume of the particle, η is the dynamic viscosity of the carrier liquid, and T is the temperature. At temperatures below the freezing point of the carrier liquid, the particles are immobilized, and in that case relaxation of the particle magnetic moment can take place only by rotation of the moment within the particle. Relaxation time for this rotation, known as the Néel relaxation, is

$$\tau_N = \tau_0 \exp\left(\frac{E}{k_BT}\right), \quad (2)$$

where τ_0 is the characteristic time of the system.

Up to now, the research attention has been focused mainly on magnetic properties and magnetic relaxation in ferrofluids with iron oxide nanoparticles (NPs) [10–15]. These materials are already in use as contrast agents for MRI and are under investigation for several other applications. On the other hand, the use of materials with larger magnetic anisotropy and larger magnetic moment is considered since it may allow the reduction of particle size. The bulk cobalt ferrite is a magnetic material with almost the same saturation magnetization as the bulk iron oxide Fe_3O_4, but with one order of magnitude higher magnetocrystalline anisotropy compared to magnetite. Because of these properties the cobalt ferrite nanoparticle systems are promising materials for high-density magnetic recording media and also very interesting for various biomedical applications [16–20]. In this work, we have synthesized $CoFe_2O_4$ NPs in an organic carrier liquid. Microstructure, morphology, and static and dynamic magnetic properties of the prepared nanomaterial were studied using X-ray diffraction (XRD), transmission electron microscopy (TEM), dynamic light scattering (DLS), Fourier-transform infrared (FTIR) spectroscopy, differential scanning calorimetry (DSC), *dc* magnetization, *ac* susceptibility measurements, and Mössbauer spectroscopy. We found that the properties of this NPs system correspond to ferrofluids: it is stable for months, magnetic nanoparticles do not agglomerate and have reproducible magnetic properties. Its main characteristics are high saturation magnetization at low temperatures close to that of the bulk material and superparamagnetic properties of most of the $CoFe_2O_4$ nanoparticles at room temperature.

2. Experimental Details

2.1. Synthesis. Synthesis of the $CoFe_2O_4$ nanoparticles was carried out via the polyol route using Co(II) acetate, Fe(III) acetonylacetonate, and diethylene glycol (DEG) from Aldrich Chemical Co as starting materials. These precursors were taken in stoichiometric ratio for obtaining the $CoFe_2O_4$ phase: 22.3775 g Fe(III) acetonylacetonate and 7.8870 g Co(II) acetate were mixed as solutions inside of diethylene glycol solvent which has been previously divided in two parts, the first volume of 150 mL for dissolution of Fe(III) acetonylacetonate and the second volume of 50 mL for dissolution of Co(II) acetate. The mixture of both solutions was magnetically stirred under the flow of nitrogen. After that, the space of the vessel filled with nitrogen was closed and the mixture was heated firstly to 120°C with a heating rate of 4°C per minute, and then the temperature was increased to 160°C and maintained at this level for 3 h. Finally, the temperature was increased to 180°C and after one hour was abruptly lowered with a high cooling rate by cold water introduced through corresponding inlet. The water flowed with a high flux around the working volume of the vessel causing a fast change of temperature from the top temperature to the room temperature. The particle solution was filtered to exclude aggregates. A Vivaspin filter (polyethersulfone (PES), Vivascience Sartorius, Hannover, Germany) with pore size 0.2 μm was used and the filtering process was performed by centrifuging the sample at 1750 rpm for about 30 min until all fluid had passed the filter. Besides the liquid sample, a powder sample was also prepared by drying the suspension of $CoFe_2O_4$ NPs at 200°C for 10 h.

2.2. Experimental Technique. X-ray characterization of the sample was carried out on a Philips PW 1050 powder diffractometer using Cu Kα radiation. The X-ray diffraction (XRD) pattern was taken in the 17°–70°2θ range with a step of 0.05° at a slow scan rate of 40 s per step. For transmission electron microscopy (TEM) measurements, the sample was prepared by drying a drop of the diluted suspension on a copper-grid-supported perforated transparent carbon foil. High-resolution transmission electron microscopy (HRTEM) and energy dispersive X-ray spectroscopy (EDXS) were carried out using a field-emission electron-source transmission electron microscope JEOL 2010 equipped with an EDXS microanalysis system (LINK ISIS EDS 300) operated at 200 kV. Average Fe/Co ratio in the composition of the nanoparticles was obtained from quantification of a large number of EDXS spectra using the Oxford ISIS software. The spectra were collected from areas of the sample containing several hundreds of the nanoparticles. For the quantification of the

spectra, the $CoFe_2O_4$ ceramics were used as a standard. The relative standard deviation of the method calculated from 20 measurements of the Fe/Co ratio on the standard was found to be inside ±2.6% ($Fe/Co_{standard}$ = 1.992 ± 0.052). The size distribution of the $CoFe_2O_4$ nanoparticles was measured by dynamic light scattering (DLS) using Zetasizer Nano ZS (Malvern, UK) equipped with green laser (532 nm). Intensity of scattered light was detected at the angle of 173°. All measurements were conducted at room temperature. Ten measurements were performed for each sample. All data processing was done by the Zetasizer software 6.20 (Malvern instruments). The size distribution is reported as distribution by number. Fourier-transform infrared (FTIR) transmission spectrum was taken at room temperature on a Perkin-Elmer 983 G spectrophotometer in the range 600–3900 cm^{-1}. Differential scanning calorimetry (DSC) measurements were performed using Setaram 151 R (softer SETSOFT 2000) instrument in the temperature range 150–240 K under helium atmosphere. Magnetic measurements were carried out on a SQUID magnetometer (MPMS XL-5, Quantum Design) equipped with an *ac* option. Zero-field-cooled (ZFC) and field-cooled (FC) measurements of magnetization were performed at applied magnetic fields from 100 to 10000 Oe in the temperature range from 2 to 300 K. Magnetic field dependence of magnetization was measured at applied magnetic fields up to 50 kOe in the temperature range from 5 to 300 K. The *ac* magnetization measurements were made under an *ac* exciting field with amplitude of 6.5 Oe using different frequencies in the range 1–1500 Hz. ^{57}Fe Mössbauer spectrum was recorded at room temperature using a conventional transmission Mössbauer spectrometer operating in constant acceleration mode. The source was ^{57}Co in Rh matrix. Experimental data were fitted to Lorentzian absorption lines by using a least square based method. The spectrometer was calibrated using α-Fe foil at room temperature. All the isomer shifts are given relative to the center of the α-Fe spectrum.

3. Results and Discussion

3.1. Structure Analysis. Figure 1 shows the XRD pattern of dry powder sample. The diffraction peaks are consistent with those of the cubic spinel phase (space group Fd3m). The lattice parameter obtained from Rietveld analysis was found to be a = 8.390 Å. The average crystallite size determined from the width of the X-ray diffraction lines using Scherrer's formula was estimated as 5 nm.

The morphology, particle size, and chemical composition of the $CoFe_2O_4$ nanoparticles deposited from organic liquid dispersion were characterized by TEM, HRTEM, and EDXS. TEM analysis (Figure 2(a)) shows that the sample contains the nanoparticles with a narrow size distribution. The measurement of approximately 500 nanoparticles from TEM images gave equivalent diameter of 5.9 ± 1.0 nm. HRTEM imaging showed good crystallinity of the nanoparticles (Figure 2(b)). The electron diffraction pattern (inset of Figure 2(a)) corresponds to a spinel structure. The EDXS spectra analysis confirmed stoichiometric composition of the

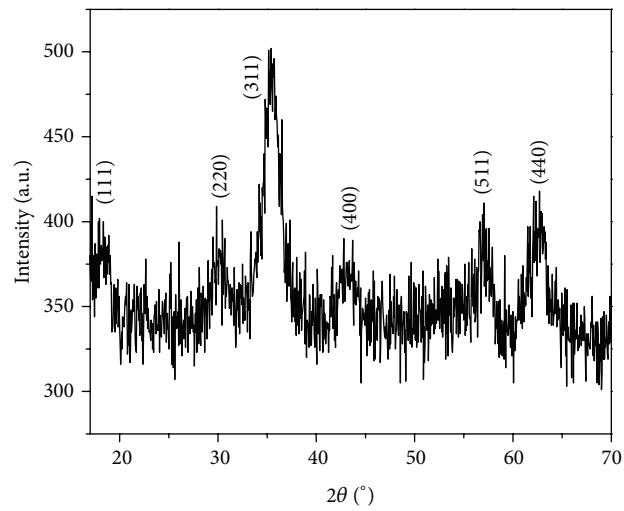

Figure 1: Powder X-ray diffraction pattern of the $CoFe_2O_4$ dried powder sample indexed with the *(hkl)* reflections of the cubic spinel.

cobalt ferrite nanoparticles in the margins of the experimental uncertainty. The measured Fe/Co ratio was 2.08 ± 0.14.

The size distribution of the $CoFe_2O_4$ nanoparticles in the organic liquid was studied using dynamic light scattering (DLS). The result is presented in Figure 3. Measured number of particles as a function of hydrodynamic particle diameter can be well described by a log-normal distribution:

$$f(d) = \frac{1}{\sqrt{2\pi}\sigma d} \exp\left[-\frac{\ln^2(d/d_0)}{2\sigma^2}\right]. \quad (3)$$

The best fit yields the distribution width σ = 0.22 and median of the distribution d_0 = 14.1 nm related to the average hydrodynamic diameter $d_{av} = d_0 \exp(\sigma^2/2)$ = 14.4 nm. The hydrodynamic diameters are larger than those measured by TEM. This is because DLS measures the size of the particles together with organic shell which cannot be observed in the TEM images due to poor contrast with respect to the background as a result of low electron density of the organic structure. Difference between the average hydrodynamic diameter of the particles and equivalent TEM diameter gives a measure of the thickness of the organic shell. The organic shell thickness thus estimated is about 4 nm.

FTIR transmission spectrum of the organic liquid suspension of $CoFe_2O_4$ NPs was measured at room temperature in the region from 600 to 3900 cm^{-1} (Figure 4). The band at 2350 cm^{-1} can be assigned to (Co, Fe)-OH vibrations caused by the interaction of the $CoFe_2O_{4-x}(OH)_x$ surface layer of the nanoparticles with polar group chains of the diethylene glycol (DEG). Almost negligible band at 2331 cm^{-1} belongs probably to the symmetric stretching mode of the ν_s CH_2. The band at 1625 cm^{-1} belongs to the ν_s (COO^-) asymmetric stretching mode of carboxyl acids. A slightly pronounced band at 1316 cm^{-1} belongs to the C-O-C stretching vibrations inside of residual DEG chains [17, 21]. The slightly pronounced band arising from the residual DEG chains with missing other characteristic bands for DEG at 1050 and 1080 cm^{-1} shows

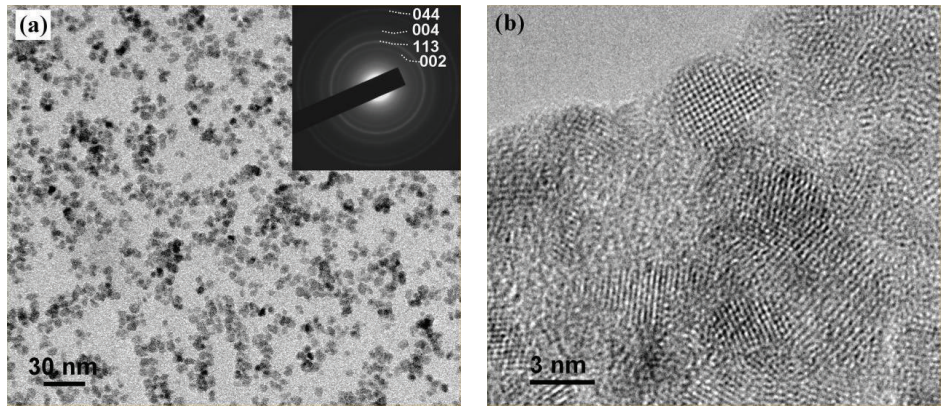

(a) (b)

Figure 2: TEM (a) and HRTEM (b) images of the $CoFe_2O_4$ nanoparticles. Electron diffraction pattern in the inset of Figure 2(a) was indexed according to the spinel structure.

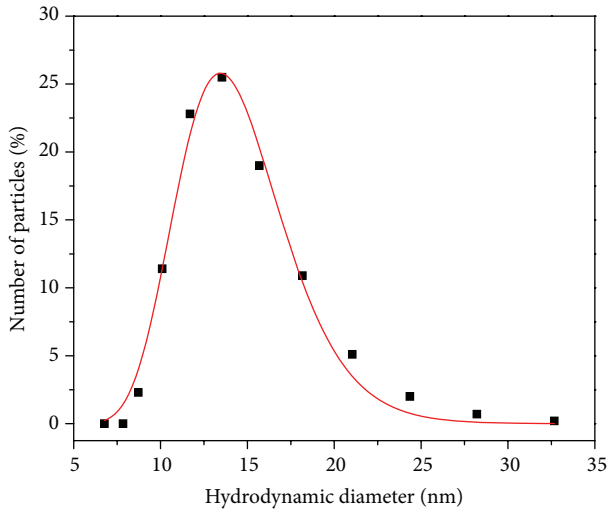

Figure 3: Hydrodynamic size distribution of the $CoFe_2O_4$ nanoparticles suspended in the organic liquid measured by dynamic light scattering. The solid curve is the fit of the dependence (3) to the experimental data.

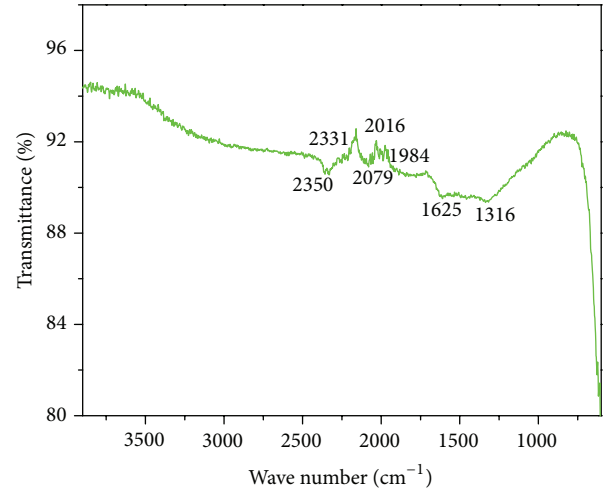

Figure 4: Fourier-transform infrared transmission spectrum of the organic liquid suspension of $CoFe_2O_4$ nanoparticles at room temperature.

that DEG is mostly changed probably into diethylene glycol acetate (ester compound) and diethylene glycol acetonylacetonate. The band at 2350 cm^{-1} proves the existence of significant interaction between the $CoFe_2O_{4-x}(OH)_x$ surface layer of the nanoparticles and organic shell. It can be noticed also that a very small fraction of DEG remained unreacted due to excess of DEG compared to carboxyl acid groups inside of starting mixture for the synthesis of the organic liquid suspension of $CoFe_2O_4$ NPs.

3.2. Magnetic Properties

3.2.1. dc Magnetization. The temperature dependence of zero-field-cooled and field-cooled magnetization curves for the organic liquid suspension of $CoFe_2O_4$ NPs was measured at applied magnetic fields from 100 to 10000 Oe. The concentration of the $CoFe_2O_4$ phase in the liquid sample was 0.045 g/mL which corresponds to the volume fraction of 0.84%. Magnetization values are expressed per unit mass of $CoFe_2O_4$ taking into account the mass fraction of the $CoFe_2O_4$ nanoparticles in the liquid. The representative ZFC-FC curves for several selected magnetic field values are shown in Figure 5. To explore possible aging effects, we compared these measurements with the previous runs performed several months ago. Measured magnetizations were reproduced within a few percent of precision. As can be seen, the ZFC and FC magnetizations of the liquid sample bifurcate at a certain temperature and show a broad peak in the ZFC curve with a maximum at temperature T_{max}. The broad peak in the ZFC magnetization is characteristic of superparamagnetic nanoparticles with size distribution where the temperature of the maximum T_{max} represents the average blocking temperature. The temperature T_{max} for the

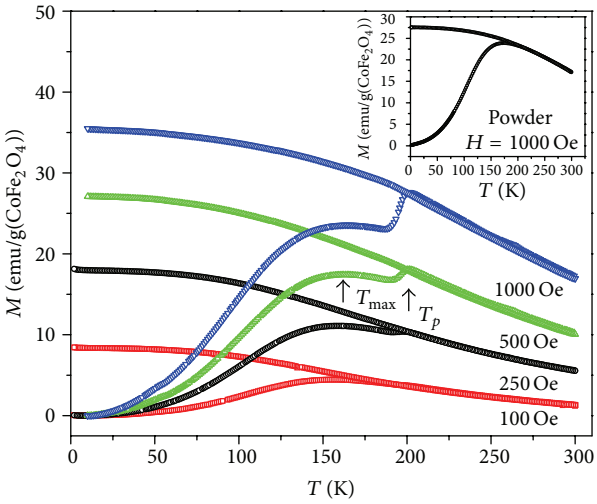

FIGURE 5: Temperature dependence of the zero-field-cooled (ZFC) and field-cooled (FC) magnetization curves for the organic liquid suspension of $CoFe_2O_4$ nanoparticles at several selected magnetic field values. The inset shows the temperature dependence of the ZFC-FC magnetization of dry powder at $H = 1000$ Oe.

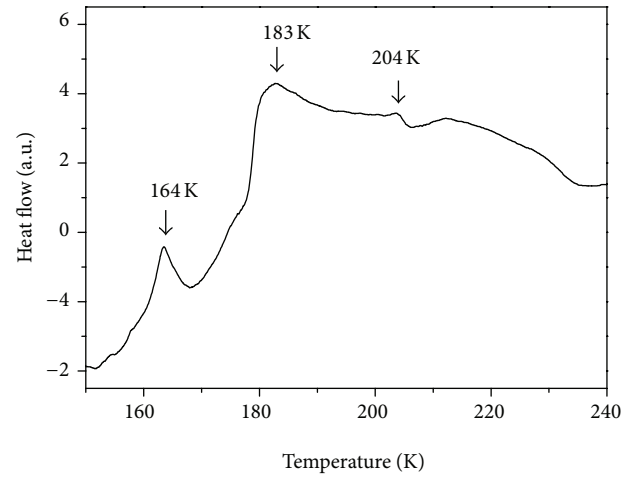

FIGURE 6: Differential scanning calorimetry curve for the liquid sample of the $CoFe_2O_4$ nanoparticles in the temperature range 150–240 K.

liquid sample extends in the range 156–164 K depending on the magnetic field values in the range $H \leq 1000$ Oe. Besides the broad peak in the ZFC magnetization, a cusp at about $T_p \approx 200$ K was also detected, which can be clearly seen for magnetic fields $H \geq 500$ Oe (Figure 5).

In order to get some insight into the origin of the cusp in the ZFC magnetization of the organic liquid suspension of $CoFe_2O_4$ NPs at about 200 K, we have measured the ZFC-FC magnetization of dry powder at $H = 1000$ Oe which is shown in the inset of Figure 5. As can be seen, there is no cusp in the ZFC magnetization of the powder sample in contrast to the liquid sample where this cusp is clearly observed. This finding suggests that the origin of the cusp in the ZFC magnetization of the liquid sample at about 200 K is associated with the carrier liquid. We performed differential scanning calorimetry (DSC) measurements on the liquid sample and the result is presented in Figure 6. Three distinct peaks in DSC graph were found. The first peak at about 204 K indicates the temperature where a part of the organic liquid enters the frozen or so called mixed state [11]. The second peak at about 183 K probably is due to freezing of the remaining part of the organic liquid. The peak at about 164 K indicates transition temperature of the liquid from the partly frozen (mixed) state to the completely frozen (solid) state. It can be noticed that the temperature of the cusp observed in the ZFC magnetization at about $T_p \approx 200$ K is just below the temperature 204 K where the organic liquid enters the frozen state. The fact that the magnetization of the magnetic nanoparticles dispersed in the liquid is sensitive to the Brownian motion of the particles in that liquid and that there is no anomalous behavior of the magnetization in the dry powder gives evidence that the cusp in the ZFC magnetization of the organic liquid suspension of $CoFe_2O_4$ NPs is due to the freezing of the organic liquid.

The magnetic field dependence of magnetization for the suspension of the $CoFe_2O_4$ NPs at $T = 5$ K and 300 K is presented in Figure 7. The $M(H)$ curve at $T = 300$ K exhibits superparamagnetic behavior: the coercive field H_c and remanent magnetization M_r are zero and the saturation magnetization, estimated by extrapolation of the M versus $1/H$ curve in the limit $1/H \to 0$, is 50.1 emu/g ($CoFe_2O_4$). For comparison, saturation magnetization of the bulk $CoFe_2O_4$ at 300 K is M_s (bulk) ≈ 76 emu/g [22]. At $T = 5$ K, the liquid sample exhibits hysteresis loop. The $M(H)$ measurements carried out at magnetic fields in the range of ±50 kOe gave $H_c = 11.8$ kOe, $M_r = 39.1$ emu/g($CoFe_2O_4$), and $M_s = 80.8$ emu/g($CoFe_2O_4$) which was estimated also by the extrapolation of the M versus $1/H$ dependence in the limit $1/H \to 0$. The saturation magnetization at $T = 5$ K falls into the region of the M_s values for the bulk $CoFe_2O_4$ ranging from 80 to 94 emu/g [23]. The saturation magnetization of the $CoFe_2O_4$ NPs in the liquid sample at 5 K, as well as that at room temperature, is considerably higher than that for the $CoFe_2O_4$ NPs obtained by either thermal decomposition [24, 25], or microemulsion route [26], or mechanical milling [27]. It appears that the method of synthesis applied in the present work favors good crystallinity and magnetic ordering resulting in a high saturation magnetization.

Saturation magnetization of 80.8 emu/g($CoFe_2O_4$) for the $CoFe_2O_4$ NPs in the liquid sample at $T = 5$ K corresponds to $\mu_s = 3.4\mu_B$ per unit chemical formula which is only slightly larger than that for inverse spinel ($3\mu_B$). Utilizing the formula $(Co_{1-\delta}Fe_\delta)[Co_\delta Fe_{2-\delta}]O_4$ to describe the cation distribution in the spinel structure of the $CoFe_2O_4$ nanoparticles, where δ is the inversion parameter, and assuming that Fe^{3+} and Co^{2+} ions have a magnetic moment of $5\mu_B$ and $3\mu_B$, respectively, we find that $\delta = 0.91$. The value of the inversion parameter δ indicates that the crystal structure of the $CoFe_2O_4$ NPs is very close to the inverse spinel.

Coercive field and saturation magnetization of the liquid sample as a function of temperature are presented in the

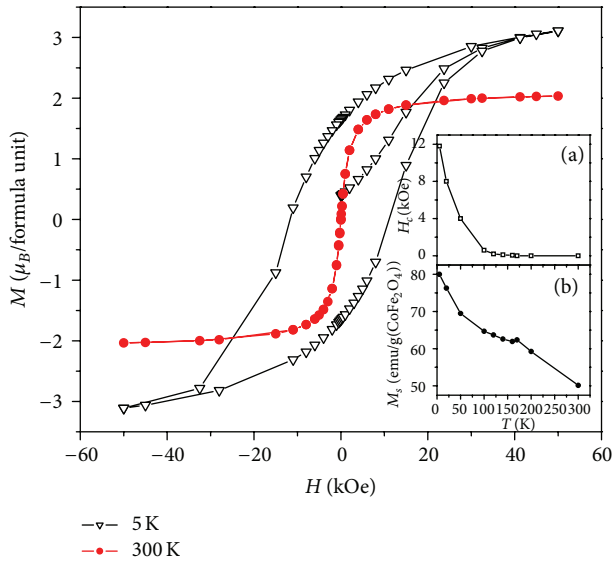

FIGURE 7: Magnetic field dependence of the magnetization for the organic liquid suspension of the $CoFe_2O_4$ nanoparticles at 5 K and 300 K. The inset shows the temperature dependence of (a) coercive field and (b) saturation magnetization.

inset of Figure 7. The coercive field decreases with increasing temperature and vanishes at about 170 K. The saturation magnetization exhibits specific properties. First, there is a small kink in the M_s versus T plot at 170 K where the coercive field vanishes, and, second, the character of the function $M_s(T)$ is changed at this temperature. Remanent magnetization (not shown) also decreases with increasing temperature and vanishes at about 170 K.

The broad peak in the ZFC magnetization at $T_{\max}$ extending from 156 to 164 K for the magnetic field in the range $H \leq 1000$ Oe as well as the disappearance of the coercive field and remanent magnetization at about 170 K suggests that a large fraction of the $CoFe_2O_4$ nanoparticles in the organic liquid are subject to the blocking process at temperatures below 170 K.

3.2.2. ac Magnetic Susceptibility. Figure 8 shows the temperature dependence of (a) the real part χ' and (b) the imaginary part χ'' of the *ac* magnetic susceptibility for the suspension of the $CoFe_2O_4$ NPs at different frequencies in the range 1–1500 Hz. It can be seen that the real component χ' has a maximum at a temperature T_{m1} in the vicinity of 200 K which shifts towards higher temperatures with increasing frequency. The imaginary part χ'' has a maximum at a temperature T_{m2} around 160 K which also shifts towards higher temperatures with increasing frequency. This property is not only characteristic of most of the spin glass systems but also of the interacting and noninteracting superparamagnetic nanoparticles. It should be noticed that the temperature T_{m1} falls into the temperature region of freezing of the organic liquid, while T_{m2} falls into the temperature region of the broad peak in the ZFC magnetization of the liquid sample. In fact, the temperature T_{m2} is significantly lower than the temperatures around 200 K where the organic liquid enters the frozen (mixed) state. Therefore, we could expect that at T_{m2} the particles are mainly frozen and cannot move, and relaxation of the particle magnetic moments in that case should occur relative to the particle through the Néel relaxation.

According to Néel [28] magnetic moment of noninteracting single domain particles with uniaxial magnetic anisotropy relaxes via an activated process, $\tau = \tau_0 \exp(E/k_BT)$, that is, the Arrhenius law, where E is the barrier due to anisotropy energy required for reversal of magnetic moment orientation and τ is the relaxation time. At temperatures where the relaxation time is comparable with the experimental time scale, the spins will seem to be frozen. Thus, the blocking temperature depends on the relaxation time $\tau \sim 1/f$, where f is the frequency of the experiment. We assume that the temperature of the maximum in χ'' is the blocking temperature of the $CoFe_2O_4$ particle magnetic moments. Taking $\tau = 1/2\pi f$, the relation between T_{m2} and frequency f is $f = f_0 \exp(-E/k_BT_{m2})$, where $f_0 = 1/2\pi\tau_0$. We find that T_{m2} can be fitted to the Arrhenius law. However, the fitted parameters are large or even have unphysical values: $\tau_0 = 1/2\pi f_0 = 2.9 \times 10^{-18}$ s and $E/k_B = 5360$ K.

In the further analysis, we take the interparticle interactions into account and describe the relaxation time of the particles in the vicinity of the temperature T_{m2} by the Vogel-Fulcher law,

$$\tau = \tau_0 \exp\left[\frac{E}{k_B(T - T_0)}\right], \quad (4)$$

where E is the energy barrier and the parameter T_0 depends on the interparticle interactions [11]. Now, the relation between T_{m2} and frequency f is $f = f_0 \exp[-E/k_B(T_{m2} - T_0)]$. A good fit of the Vogel-Fulcher law, (4), to the experimental data $\ln f$ versus $T_{m2}(f)$ is obtained with physically meaningful parameters, and the result is shown in Figure 9. The best fit yields $f_0 = (1.6 \pm 0.3) \times 10^{11}$ Hz, $\tau_0 = 1/2\pi f_0 = (1.0 \pm 0.3) \times 10^{-12}$ s, $E/k_B = (2300 \pm 300)$ K and $T_0 = (46.5 \pm 5)$ K. The parameter T_0 presents the average value of the interparticle interactions observed in the $\chi''(T)$ dependence in the measured frequency range. In the case of axial magnetocrystalline anisotropy, the energy barrier of superparamagnetic particles is related to the anisotropy constant, $E = KV$. For $E/k_B = 2300$ K and average volume of the particles assuming spherical geometry $\langle V \rangle = 1.075 \times 10^{-19}$ cm^3, $K = 3 \times 10^6$ erg/cm^3, which is somewhat larger than that in the bulk material [23]. High saturation magnetization of the synthesized $CoFe_2O_4$ NPs with a narrow size distribution in combination with superparamagnetic properties observed at room temperature makes these particles, with appropriate coating and functionalization, very promising materials for biomedical applications, especially in magnetic targeted drug delivery and in magnetic fluid hyperthermia.

Temperature of the maximum in the real part of the *ac* magnetic susceptibility T_{m1} appears in the vicinity of 200 K, Figure 8(a), that is, in the region where the organic liquid enters the frozen (mixed) state. In the mixed state, the system is not yet a rigid solid and the nanoparticles

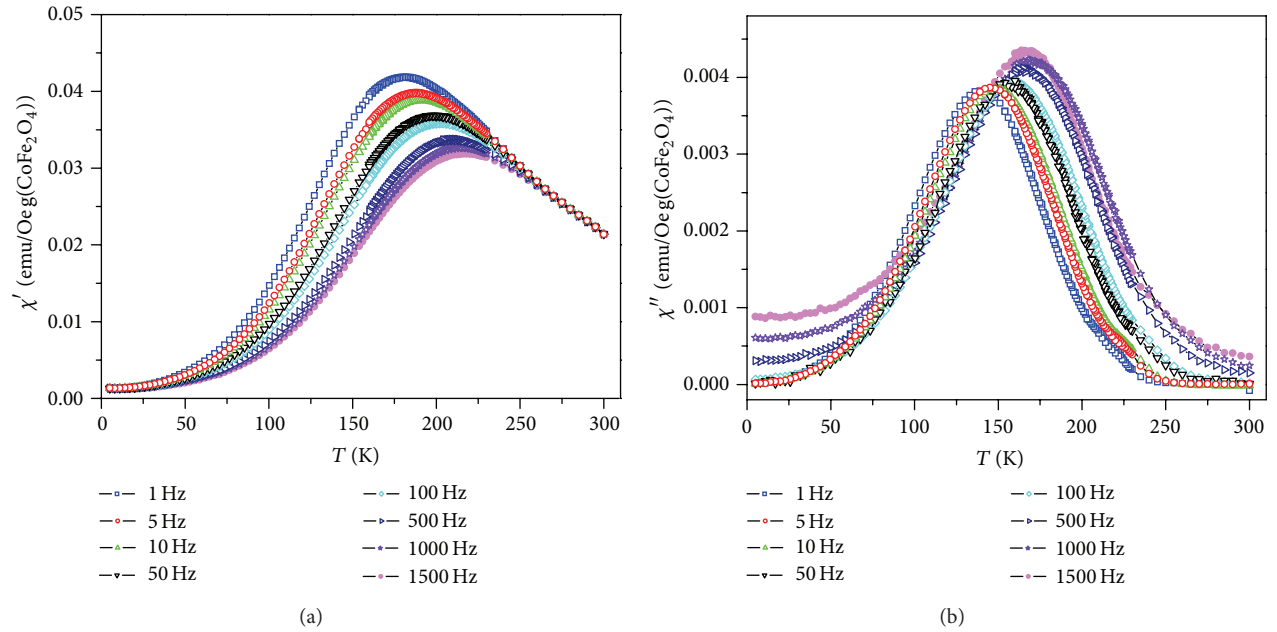

FIGURE 8: Temperature dependence of (a) the real part χ' and (b) the imaginary part χ'' of the *ac* magnetic susceptibility for the organic liquid suspension of the $CoFe_2O_4$ nanoparticles at different frequencies in the range 1–1500 Hz.

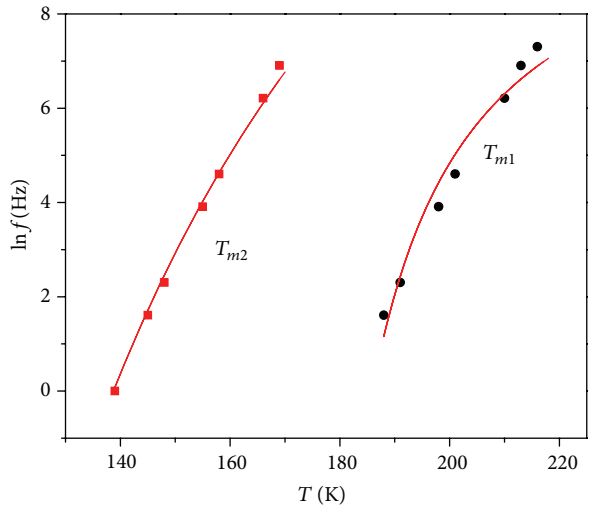

FIGURE 9: Frequency dependent temperature T_{m1} of the maximum in the real part χ' and temperature T_{m2} of the maximum in the imaginary part χ'' of the *ac* magnetic susceptibility. The solid curves represent fit of the Vogel-Fulcher law, (4), to the experimental data.

are free to move locally. Brownian relaxation arises as a response of the nanoparticles magnetic moments to the external magnetic field through the particle movement. The Vogel-Fulcher law was found to describe successfully the Brownian relaxation in the ferrofluids containing magnetite nanoparticles [11, 15]. The exponential temperature dependence of τ_B is attributed to divergence of the viscosity of the liquid at the characteristic temperature T_0', as found in many glass-forming liquids [29]. Using the Brownian relaxation time in the form $\tau_B = \tau_0' \exp[E'/k_B(T - T_0')]$, the relation between T_{m1} and frequency f is $f = f_0' \exp[-E'/k_B(T_{m1} - T_0')]$. We find that the Vogel-Fulcher law can be fitted to the experimental data $\ln f$ versus $T_{m1}(f)$ with the following parameters: $\tau_0' = 1/2\pi f_0' = (2.6 \pm 1.0) \times 10^{-6}$ s, $E'/k_B = (2.0 \pm 0.2) \times 10^2$ K, and $T_0' = (168 \pm 10)$ K. The result of this fit is shown also in Figure 9. Difference between the parameters in the Vogel-Fulcher law describing the Néel relaxation and the Brownian relaxation can be seen immediately. The characteristic time of the system τ_0' in the Brownian relaxation is much larger than τ_0 in the Néel relaxation. The large difference between the parameters E' associated with the viscosity of the liquid [11] and E in the Néel relaxation also indicates different nature of the two relaxations. The parameter T_0' should correspond to the temperature of the divergence of the viscosity, that is, to the temperature where the organic liquid passes from the partly frozen (mixed) state to the completely frozen (solid) state. It is interesting to note that $T_0' = 168$ K obtained from the Vogel-Fulcher expression for the Brownian relaxation time as a fitting parameter is in good agreement with $T = 164$ K identified as transition temperature from the mixed state to the solid state of the organic liquid recorded in the DSC measurements.

3.2.3. Mössbauer Spectroscopy. ^{57}Fe Mössbauer measurement was performed on the $CoFe_2O_4$ nanoparticles with average particle size of 5.9 nm. The experimental spectrum collected at room temperature is presented in Figure 10. The main contribution to the spectrum belongs to a quadrupolar doublet characteristic of a paramagnetic compound showing that the quadrupole interaction is much stronger than the magnetic hyperfine interaction. This quadrupolar doublet is ascribed to

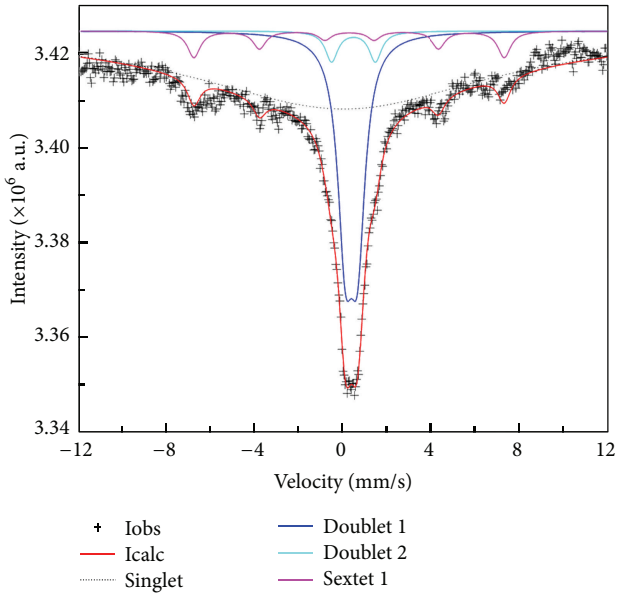

FIGURE 10: Mössbauer spectrum of the $CoFe_2O_4$ nanoparticles in the dried powder sample at room temperature.

the superparamagnetic $CoFe_2O_4$ nanoparticles. Besides the quadrupolar doublet, a six-line hyperfine pattern of lower intensity was also recorded. The presence of both the doublets and sextets in the Mössbauer spectrum is usually detected in an assembly of ultrafine particles with a size distribution. The Mössbauer spectrum of the $CoFe_2O_4$ powder sample has been fitted as a superposition of a broad singlet, two quadrupolar doublets, and one sextet. The broad singlet is introduced to delineate process of magnetic relaxations in some grains due to the particle size distribution. The isomer shift values of two doublets, (0.34 ± 0.01) mm/s and (0.43 ± 0.06) mm/s, indicate the presence of the Fe^{3+} ions in two different local environments. The quadrupolar splitting values of these doublets are (0.55 ± 0.03) mm/s and (1.98 ± 0.19) mm/s, respectively. Therefore, both doublets are assigned to the Fe^{3+} ions, one located in the particle core and the other located at the particle surface. The doublet with more positive isomer shift (0.43 mm/s) and higher quadrupolar splitting (1.98 mm/s) can be ascribed to the iron ions located at the surface layer of the particles. The hyperfine field is obtained as $B_{hyp} = (437 \pm 1)$ kOe. This hyperfine field is somewhat lower than the minimal value of the B-site hyperfine field found in the bulk cobalt ferrite [30]. Lower values of the hyperfine fields, compared to those usually reported for the cobalt ferrite nanoparticles [31, 32], were obtained to be about 440 kOe at the room temperature Mössbauer spectrum of the $CoFe_2O_4$ NPs with average diameter of 9.6 nm [33]. In a detailed analysis of the Mössbauer spectra of the $CoFe_2O_4$ NPs with average particle size of 5.1, 8.6, and 12.2 nm, acceptable fitting data were obtained only when the B-site pattern was assumed to be a superposition of more than one sextet, including those with lower hyperfine fields [27]. The Mössbauer spectrum of the $CoFe_2O_4$ powder sample studied in the present work indicates that most of the $CoFe_2O_4$ nanoparticles are superparamagnetic at room temperature, while a minor fraction of the nanoparticles have blocked magnetic moments with blocking temperatures above 300 K. Because the contribution of the $CoFe_2O_4$ particles with blocked magnetic moments is minor in the spectrum, more detailed analysis concerning the hyperfine fields is unreliable.

4. Conclusion

The synthesis procedure of the organic liquid suspension of the $CoFe_2O_4$ nanoparticles applied in the present work appears to be very promising from the aspect of the tailoring of these particles with well-pronounced magnetic properties. The narrow size distribution of the particles, high saturation magnetization, and superparamagnetic properties at room temperature make them very attractive and suitable for application in biomedicine, especially in magnetic targeted drug delivery and in magnetic fluid hyperthermia.

Acknowledgment

Financial support for this study was granted by the Ministry of Education, Science and Technological Development of Serbia (Project no. 172026).

References

[1] S. Odenbach, "Magnetic fluids—suspensions of magnetic dipoles and their magnetic control," *Journal of Physics Condensed Matter*, vol. 15, no. 15, pp. S1497–S1508, 2003.

[2] S. Odenbach, "Recent progress in magnetic fluid research," *Journal of Physics Condensed Matter*, vol. 16, no. 32, pp. R1135–R1150, 2004.

[3] C. Scherer and A. M. Figueiredo Neto, "Ferrofluids: properties and applications," *Brazilian Journal of Physics*, vol. 35, no. 3, pp. 718–727, 2005.

[4] C. C. Berry, "Progress in functionalization of magnetic nanoparticles for applications in biomedicine," *Journal of Physics D*, vol. 42, no. 22, Article ID 224003, 9 pages, 2009.

[5] H. Tan, J. M. Xue, B. Shuter, X. Li, and J. Wang, "Synthesis of PEOlated Fe_3O_4@SiO_2 nanoparticles via bioinspired silification for magnetic resonance imaging," *Advanced Functional Materials*, vol. 20, no. 5, pp. 722–731, 2010.

[6] R. Rahisuddin, P. K. Sharma, M. Salim, and G. Garg, "Application of ferrofluid: as a targeted drug delivery system in nanotechnology," *International Journal of Pharmaceutical Sciences Review and Research*, vol. 5, no. 3, pp. 115–119, 2010.

[7] R. Skomski and J. M. D. Coey, *Permanent Magetism*, Institute of Physics Publishing, Bristol, UK, 1999.

[8] M. Walker, P. I. Mayo, K. O'Grady, S. W. Charles, and R. W. Chantrell, "The magnetic properties of single-domain particles with cubic anisotropy. I. Hysteresis loops," *Journal of Physics*, vol. 5, no. 17, pp. 2779–2792, 1993.

[9] E. Blums, A. Cebers, and M. M. Maiorov, *Magnetic Fluids*, Walter de Gruyter, Berlin, Germany, 1997.

[10] T. Jonsson, J. Mattsson, C. Djurberg, F. A. Khan, P. Nordblad, and P. Svedlindh, "Aging in a magnetic particle system," *Physical Review Letters*, vol. 75, no. 22, pp. 4138–4141, 1995.

[11] J. Zhang, C. Boyd, and W. Luo, "Two mechanisms and a scaling relation for dynamics in ferrofluids," *Physical Review Letters*, vol. 77, no. 2, pp. 390–393, 1996.

[12] A. Skumiel, A. Józefczak, T. Hornowski, and M. Labowski, "The influence of the concentration of ferroparticles in a ferrofluid on its magnetic and acoustic properties," *Journal of Physics D*, vol. 36, no. 24, pp. 3120–3124, 2003.

[13] M. Blanco-Mantecón and K. O'Grady, "Interaction and size effects in magnetic nanoparticles," *Journal of Magnetism and Magnetic Materials*, vol. 296, no. 2, pp. 124–133, 2006.

[14] L.-Y. Zhang, Y.-H. Dou, L. Zhang, and H.-C. Gu, "Magnetic behaviour and heating effect of Fe_3O_4 ferrofluids composed of monodisperse nanoparticles," *Chinese Physics Letters*, vol. 24, no. 2, pp. 483–486, 2007.

[15] M. B. Morales, M. H. Phan, S. Pal, N. A. Frey, and H. Srikanth, "Particle blocking and carrier fluid freezing effects on the magnetic properties of Fe_3O_4 -based ferrofluids," *Journal of Applied Physics*, vol. 105, no. 7, Article ID 07B511, 3 pages, 2009.

[16] G. Baldi, D. Bonacchi, C. Innocenti, G. Lorenzi, and C. Sangregorio, "Cobalt ferrite nanoparticles: the control of the particle size and surface state and their effects on magnetic properties," *Journal of Magnetism and Magnetic Materials*, vol. 311, no. 1, pp. 10–16, 2007.

[17] G. Baldi, D. Bonacchi, M. C. Franchini et al., "Synthesis and coating of cobalt ferrite nanoparticles: a first step toward the obtainment of new magnetic nanocarriers," *Langmuir*, vol. 23, no. 7, pp. 4026–4028, 2007.

[18] G. Baldi, G. Lorenzi, and C. Ravagli, "Hyperthermic effect of magnetic nanoparticles under electromagnetic field," *Processing and Applications of Ceramics*, vol. 3, no. 1-2, pp. 103–109, 2009.

[19] M. C. Franchini, G. Baldi, D. Bonacchi et al., "Bovine serum albumin-based magnetic nanocarrier for MRI diagnosis and hyperthermic therapy: a potential theranostic approach against cancer," *Small*, vol. 6, no. 3, pp. 366–370, 2010.

[20] V. Cabuil, V. Dupuis, D. Talbot, and S. Neveu, "Ionic magnetic fluid based on cobalt ferrite nanoparticles: influence of hydrothermal treatment on the nanoparticle size," *Journal of Magnetism and Magnetic Materials*, vol. 323, no. 10, pp. 1238–1241, 2011.

[21] H. Guo, X. Yang, T. Xiao, W. Zhang, L. Lou, and J. Mugnier, "Structure and optical properties of sol-gel derived Gd_2O_3 waveguide films," *Applied Surface Science*, vol. 230, no. 1–4, pp. 215–221, 2004.

[22] H. Shenker, "Magnetic anisotropy of cobalt ferrite ($Co_{1.01}Fe_{2.00}O_{3.62}$) and nickel cobalt ferrite ($Ni_{0.72}Fe_{0.20}Co_{0.08}Fe_2O_4$)," *Physical Review*, vol. 107, no. 5, pp. 1246–1249, 1957.

[23] V. A. Brabers, "Progress in spinel ferrite research," in *Handbook of Magnetic Materials*, K. H. J. Buschow, Ed., vol. 8, North-Holland, Amsterdam, The Netherlands, 1995.

[24] M. Grigorova, H. J. Blythe, V. Blaskov et al., "Magnetic properties and Mössbauer spectra of nanosized $CoFe_2O_4$ powders," *Journal of Magnetism and Magnetic Materials*, vol. 183, no. 1-2, pp. 163–172, 1998.

[25] V. Blaskov, V. Petkov, V. Rusanov et al., "Magnetic properties of nanophase $CoFe_2O_4$ particles," *Journal of Magnetism and Magnetic Materials*, vol. 162, no. 2-3, pp. 331–337, 1996.

[26] N. Moumen, P. Veillet, and M. P. Pileni, "Controlled preparation of nanosize cobalt ferrite magnetic particles," *Journal of Magnetism and Magnetic Materials*, vol. 149, no. 1-2, pp. 67–71, 1995.

[27] E. Manova, B. Kunev, D. Paneva et al., "Mechano-synthesis, characterization, and magnetic properties of nanoparticles of cobalt ferrite, $CoFe_2O_4$," *Chemistry of Materials*, vol. 16, no. 26, pp. 5689–5696, 2004.

[28] L. Néel, "Thermoremanent magnetization of fine powders," *Review of Modern Physics*, vol. 25, no. 1, pp. 293–295, 1953.

[29] N. Menon and S. R. Nagel, "Evidence for a divergent susceptibility at the glass transition," *Physical Review Letters*, vol. 74, no. 7, pp. 1230–1233, 1995.

[30] G. A. Sawatzky, F. van der Woude, and A. H. Morrish, "Mössbauer study of several ferrimagnetic spinels," *Physical Review*, vol. 187, no. 2, pp. 747–757, 1969.

[31] N. Moume, P. Bonville, and M. P. Pileni, "Control of the size of cobalt ferrite magnetic fluids: Mössbauer spectroscopy," *Journal of Physical Chemistry*, vol. 100, no. 34, pp. 14410–14416, 1996.

[32] A. Hutlova, D. Niznansky, J.-L. Rehspringer, C. Estournès, and M. Kurmoo, "High coercive field for nanoparticles of $CoFe_2O_4$ in amorphous silica sol-gel," *Advanced Materials*, vol. 15, no. 19, pp. 1622–1625, 2003.

[33] S. R. Ahmed, S. B. Ogale, G. C. Papaefthymiou, R. Ramesh, and P. Kofinas, "Magnetic properties of $CoFe_2O_4$ nanoparticles synthesized through a block copolymer nanoreactor route," *Applied Physics Letters*, vol. 80, no. 9, pp. 1616–1618, 2002.